Magnetically Induced Depolarization of Microwave Scattering from a Laser-Generated Plasma

C.A. Galea,[*] M.N. Shneider, A. Dogariu, and R.B. Miles[†]

Department of Mechanical and Aerospace Engineering, Princeton University, Princeton, New Jersey 08544, USA

The effects of a local external magnetic field on microwave scattering from a laser-generated plasma are investigated by modeling and experiment, leading to the prediction and observation of magnetically induced depolarization of scattered microwaves. The sample volume is localized by the small laser-generated plasma and depolarization is shown to depend on both the magnitude and direction of the magnetic field; this indicates the potential for standoff detection and measurement of vector magnetic fields in gases.

I. INTRODUCTION

In this paper, we study the effects of an external magnetic field on microwave scattering from a laser-generated plasma and demonstrate magnetically induced depolarization of the scattered microwaves. Because magnetically induced depolarization occurs locally at a small plasma and depends on both the magnitude and direction of the magnetic field, the discovery of this magneto-optical effect suggests potential technology for standoff detection and measurement of local vector magnetic fields in gases.

Historically, a variety of magneto-optical rotation effects have been studied, including Faraday rotation [1], the Kerr magneto-optic effect [2], and the Voigt effect [3]. Unlike Faraday rotation, where polarization rotation is due to propagation through an optically active medium, such as plasma [4], the interaction with a small plasma, where $\lambda \gg L_p$ ($\lambda = 2\pi c/\omega$ is the wavelength of electromagnetic radiation and L_p is the plasma length scale), can result in a magnetically induced polarization change not yet considered that is independent of propagation length. Previous theoretical investigations of electromagnetic scattering by a small plasma in a magnetic field [5–7] solved problems similar to the classic Mie problem to obtain the scattered fields, but depolarization effects were not considered. Here, we present a derivation of the magnetically induced depolarization effect and demonstrate this effect in experiments, hence introducing the capability of standoff measurements of local magnetic fields.

Shneider and Miles [8] investigated microwave scattering by small plasma objects, showing that, for a plasma with a skin depth of $\delta > L_p$, the plasma scattered radiation as an oscillating dipole. Their findings led to a new regime of microwave scattering diagnostics, including radar resonance-enhanced multiphoton ionization (Radar REMPI) [9] and Rayleigh microwave scattering (RMS) [10]. Radar REMPI is applied to trace species detection [11], electron-loss rate measurements [12], and temperature measurements in gas mixtures and flames [13–15], while RMS is applied to time-resolved measurements of electron number density for plasma medicine applications and multiphoton ionization cross-section measurements [10,16]. Both Radar REMPI and RMS achieve nanosecond time resolution through GHz bandwidth homo- or heterodyne detection. Here, we extend these methods to the time-accurate measurement of local magnetic field properties.

Magnetically induced depolarization of microwave scattering from a laser-generated plasma enables a magnetic field measurement that is localized at the small plasma and can be detected at arbitrary angles. This is in contrast to the measurement of a magnetic field via Faraday rotation, which is path integrated and requires measurement of a forward propagating beam. The measurement of a vector magnetic field via the magnetically induced depolarization effect is distinct from (but can be complementary to) remote vector magnetometers in the literature [17–20]. The proposed measurement technology brings standoff capability to magnetometry; this allows one to measure and monitor magnetic fields in environments with limited diagnostic access.

II. THEORY

To model the interaction, we consider a small plasma sphere with a length scale of L_p and assume the plasma to have a skin depth of $\delta > L_p$. We model the effects of

---

*cgalea@princeton.edu

†Also at Department of Aerospace Engineering, Texas A&M University, College Station, Texas 77843, USA
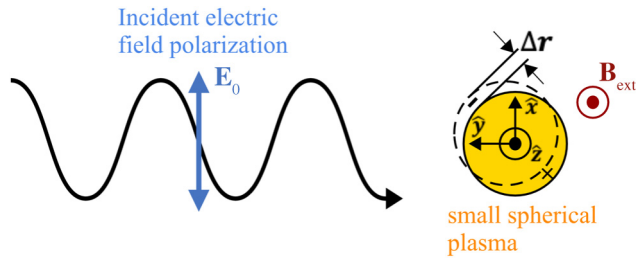
FIG. 1. Model setup for microwave scattering by small plasma in a magnetic field. A polarized incident microwave beam interacts with small spherical plasma, resulting in an oscillating induced dipole moment. $\Delta \mathbf{r}$ is the vector electron displacement from the main plasma body.

a polarized incident microwave field with an angular frequency of ω on the motion of electrons within the main plasma body in the presence of an external magnetic field, illustrated in Fig. 1. Assuming a Maxwellian distribution of electrons, a fixed background of ions, and a spatially constant density plasma of number density n and volume V, we obtain the equation of motion for a displaced electron:

$$\ddot{\Delta \mathbf{r}} = -\frac{e}{m}(\mathbf{E}_0 e^{-i\omega t} + \dot{\Delta \mathbf{r}} \times \mathbf{B}_{\text{ext}}) - \nu_m \dot{\Delta \mathbf{r}} - \zeta \omega_p^2 \Delta \mathbf{r}, \tag{1}$$

where $\Delta \mathbf{r}$ is the vector displacement of the electron, e/m is the electron charge-to-mass ratio, $\mathbf{E}_0$ is the microwave electric field amplitude, $\mathbf{B}_{\text{ext}}$ is the applied external magnetic field, ν_m is the electron momentum transfer collision frequency, and $\omega_p = \sqrt{ne^2/m\epsilon_0}$ is the plasma frequency. The depolarization factor, ζ [21], is included to capture the effect of the plasma geometry on electric polarization; since we have assumed a spherical plasma, $\zeta_x = \zeta_y = \zeta_z = \zeta = 1/3$. We neglect the Lorentz force due to the microwave magnetic field, since this is much smaller than the Lorentz force due to the microwave electric field for nonrelativistic electrons.

Taking $\mathbf{E}_0 = E_0 \hat{\mathbf{x}}$, $\mathbf{B}_{\text{ext}} = B_{\text{ext}} \hat{\mathbf{z}}$, and $\Delta \mathbf{r} = \Delta x \hat{\mathbf{x}} + \Delta y \hat{\mathbf{y}} + \Delta z \hat{\mathbf{z}}$, we obtain a coupled system of driven damped harmonic oscillators for Δx and Δy (the displacement in $\hat{\mathbf{z}}$ is unaffected by the fields in this setup). We then take $\Delta x = \Delta x_0 e^{-i\omega t}$ and $\Delta y = \Delta y_0 e^{-i\omega t}$ to obtain the nonhomogeneous solution due to the interaction with the microwave field. The complex amplitudes Δx_0 and Δy_0 are found to be:

$$\Delta x_0 = \frac{-\xi(e/m)E_0}{1 - \omega^2 \omega_c^2 \xi^2}, \tag{2}$$

and

$$\Delta y_0 = \frac{i\omega \text{sgn}(B_{\text{ext}})\omega_c \xi^2 (e/m)E_0}{1 - \omega^2 \omega_c^2 \xi^2}, \tag{3}$$

where $\omega_c = e|B_{\text{ext}}|/m$ is the electron gyrofrequency and $\xi = (\zeta \omega_p^2 - \omega^2 - i\nu_m \omega)^{-1}$. We consider small magnetic field and low collisionality limits, i.e., keeping terms to first order in (ω_c/ω) and (ν_m/ω) with $\omega_c \omega \ll |\zeta \omega_p^2 - \omega^2|$ and $\nu_m \omega \ll |\zeta \omega_p^2 - \omega^2|$, respectively. These approximations fall well within the limits of our experiments and help to more clearly illustrate the magnetic field effect. [The full expressions in Eqs. (2) and (3) need to be used if the experimental parameters do not fall within these limits.]

In the Rayleigh regime, where the receiver distance from the plasma is $R \gg \lambda \gg L_p$ and the skin depth is $\delta > L_p$ [8], the averaged scattered dipole radiation power is [22]:

$$\langle \Theta \rangle = \frac{|\ddot{\mathbf{d}}|^2}{6\pi \epsilon_0 c^3}, \tag{4}$$

where $\mathbf{d} = enV\Delta \mathbf{r}$ is the induced dipole moment of the small plasma. Using the principle of superposition, we can obtain the scattered electric field signal, E_s (the measurable quantity in microwave scattering experiments), in the $\hat{\mathbf{x}}$ and $\hat{\mathbf{y}}$ polarizations by considering the induced dipole moment for each polarization independently:

$$E_{sx} \propto \sqrt{\langle \Theta_x \rangle} \propto |\Delta x_0|, \tag{5}$$

and

$$E_{sy} \propto \sqrt{\langle \Theta_y \rangle} \propto |\Delta y_0|, \tag{6}$$

which gives the depolarization ratio:

$$\frac{E_{sy}}{E_{sx}} = \frac{1}{\sqrt{\left[1 - \zeta \left(\frac{\omega_p}{\omega}\right)^2\right]^2 + \left(\frac{\nu_m}{\omega}\right)^2}} \left(\frac{\omega_c}{\omega}\right). \tag{7}$$

The phase difference, $\Delta \varphi$, between $\hat{\mathbf{x}}$ and $\hat{\mathbf{y}}$ polarization scattered fields is found from the phase difference between Δx_0 and Δy_0:

$$\tan \Delta \varphi = \frac{1 - \zeta \left(\frac{\omega_p}{\omega}\right)^2}{\left(\frac{\nu_m}{\omega}\right)}. \tag{8}$$

The angular dependence of scattered electric field polarizations follows from the corresponding radiation patterns for the oscillating dipoles in each polarization direction [8]; we consider scattering in the $\hat{\mathbf{z}}$ direction because $\hat{\mathbf{x}}$ and $\hat{\mathbf{y}}$ dipoles both radiate at a maximum in this direction. We draw two conclusions based on this model: (1) in the presence of a magnetic field, we obtain a magnetically induced depolarization (in the $\mathbf{E}_0 \times \mathbf{B}_{\text{ext}}$ direction) of microwave scattering, and (2) this depolarization signal is linear in
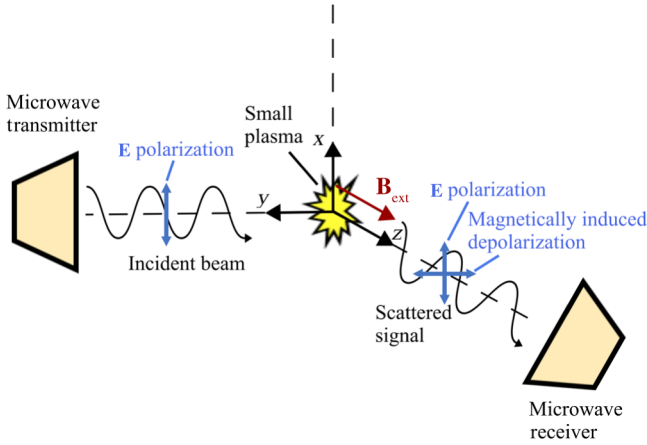
FIG. 2. Illustration of the magnetically induced depolarization effect. The incident microwave beam is polarized in the **E** polarization direction. The scattering in a magnetic field leads not only to **E** polarization, but also to a magnetically induced depolarization component.

$\omega_c \propto B_{\text{ext}}$ to first order. Reversing the direction of B_{ext} results in a $180°$ phase shift in the depolarization signal, which can be seen from the $\text{sgn}(B_{\text{ext}})$ term in Eq. (3). The magnetically induced depolarization of the scattering signal is illustrated in Fig. 2.

The physical mechanism behind magnetically induced depolarization can be pictured as follows: An incoming microwave beam with an initial polarization (**E** polarization) is scattered by plasma electrons in the presence of an external magnetic field. The electrons will have an oscillation component in the **E** polarization direction at microwave frequency, acting as an oscillating dipole that radiates **E** polarization, but will also experience an **E** × B_{ext} drift, which oscillates at the same frequency. This results in an oscillating dipole component in the **E** × B_{ext} direction, and hence, radiation of **E** × B_{ext} polarization, which is orthogonal to **E** polarization and is referred to as "magnetically induced depolarization." Note that the derivation of the full tensor linking $\mathbf{E}_s (\propto \Delta\mathbf{r})$ and arbitrary $\mathbf{E}_0$ is a simple extension of the model introduced here to the cases $\mathbf{E}_0 = E_0\hat{\mathbf{y}}$ and $\mathbf{E}_0 = E_0\hat{\mathbf{z}}$, where the former also demonstrates the magnetically induced depolarization effect, while the latter is equivalent to zero external magnetic field, since, in this case, $\mathbf{E}_0 \parallel \mathbf{B}_{\text{ext}}$. By applying a rotation matrix to this tensor, we can then find the expected scattering polarization ratios for an arbitrary magnetic field orientation, which can then be used to measure the vector magnetic field. If the plasma is generated by laser-induced ionization at a laser focus, the measurements can be spatially resolved and, since microwave scattering is used to probe this small laser-generated plasma, one can perform standoff measurements of the local vector magnetic field.

III. EXPERIMENT SETUP

The experiment setup follows from the illustration in Fig. 2. The small plasma ($L_p \approx 0.1$ mm) is produced via 2+1 REMPI of xenon by focusing a 0.2 mJ, 1 kHz repetition rate, 100 fs laser pulse at a wavelength of 256 nm, with a lens of 30 cm focal length into a quartz glass cell of 7 mTorr xenon with fused silica windows. The external magnetic field is generated by an electromagnet with a maximum magnetic field of $B_{\text{max}} \approx 0.08$ T. The bistatic homodyne microwave detection system is described in Ref. [10]. The transmitter emits $\omega/2\pi = 12.6$ GHz microwaves with **E** polarization, which are scattered by the plasma ($\lambda = 2.38$ cm $\gg L_p$ ensures the plasma can be considered small). The receiver can be rotated to select either the scattered **E** polarization or **E** × B_{ext} polarization, the resulting signals of which are the **E** polarization and magnetically induced depolarization (also referred to as "depolarization") signals, respectively. The transmitter and receiver are both at a distance $R \approx 10$ cm away from the laser-generated plasma. We also have $\delta \approx 3$ mm, along with the relevant characteristic frequencies, $\omega_c/2\pi \approx 2$ GHz, $\nu_m \approx 2$ GHz, and $\omega_p/2\pi \approx 100$ GHz, ensuring that our experiment satisfies the Rayleigh regime, as well as the small magnetic field and low collisionality limits described above. To ensure the plasma does not distort the external magnetic field, we require the magnetic Reynolds number, $R_m = UL\mu_0\sigma$, to be less than unity, where U is the plasma fluid velocity, L is the magnetic field gradient length scale, and σ is the plasma conductivity [23]. For the small plasma in our experiment (which expands via ambipolar diffusion), we have as upper bound estimates $U \approx 20$ km/s, $L \approx 1$ mm, and $\sigma \approx 3000$ Ω^{-1} m^{-1}, which result in $R_m \approx 0.06 \ll 1$. For the preceding calculations, the electron temperature, $T_e \approx 2$ eV, is estimated by calculating excess energy above the ionization threshold to which the three-photon ionization (from 2+1 REMPI) process contributes, and dividing this excess energy among the three degrees of freedom of the newly freed electron. We also use the upper bound on the plasma density, $n \approx 3 \times 10^{20}$ m^{-3} (full ionization case), to ensure a maximum estimate for the magnetic Reynolds number.

IV. RESULTS AND DISCUSSION

The effect of switching on an external magnetic field of $B_{\text{ext}} = B_{\text{max}}$ is shown in Fig. 3 for both depolarization and **E** polarization signals. Notably, (1) there is a nonzero depolarization scattering signal for $B_{\text{ext}} = 0$ due to other depolarization effects (such as scattering by the glass cell and randomly oriented nuclear spins); and (2) there is a small phase shift between the depolarization and **E** polarization setups, leading to a qualitative difference in the signals. Neither of these points are issues in our test, since we focus on the relative change due to the introduction of
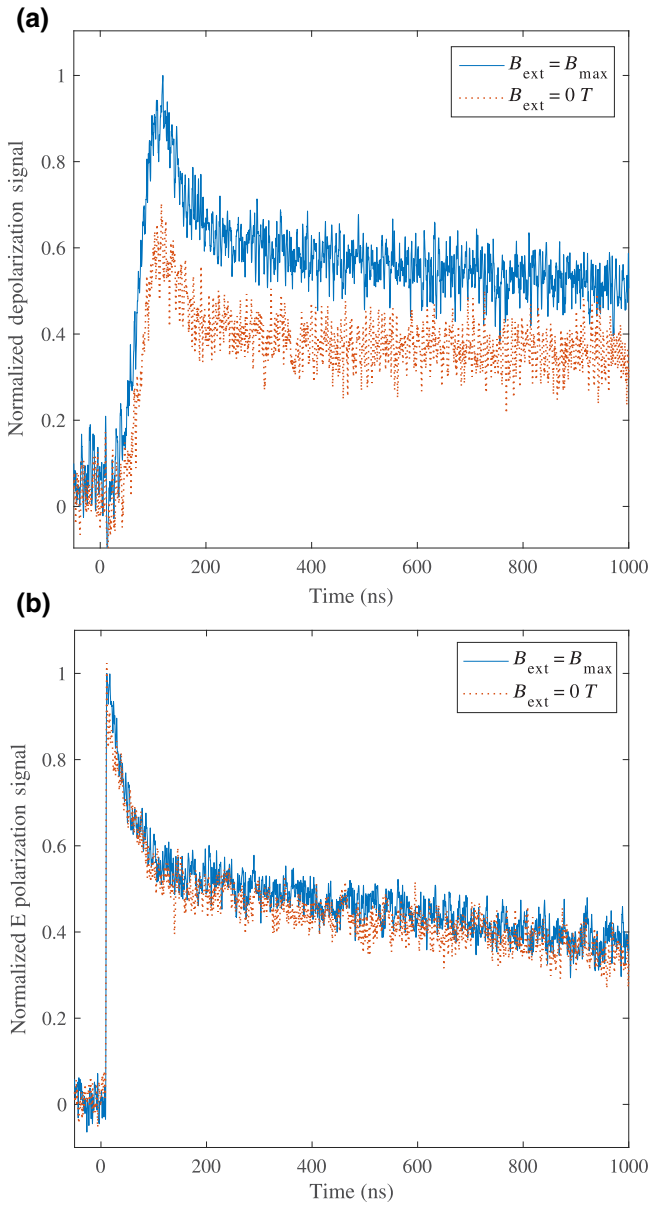
(a)

(b)

FIG. 3. Microwave scattering signal at maximum and zero external magnetic fields for (a) magnetically induced depolarization and (b) **E** polarization. The magnetically induced depolarization signal has a greater relative change than that of the **E** polarization signal, which agrees with our model. The results are averaged over 1000 laser shots.

an external magnetic field in each case. The magnetically induced depolarization signal has a greater relative change than that of the **E** polarization signal, which is in agreement with our model: the depolarization signal is proportional to $(\omega_c/\omega) \approx 1/6$ [Eq. (6)], while the **E** polarization signal has no dependence on the magnetic field [Eq. (5)], since the effect is of second order, i.e., $(\omega_c/\omega)^2 \approx 1/36 \ll 1$. These findings suggest adjusting the receiver to the **E** polarization to perform measurements of quantities described in Refs.
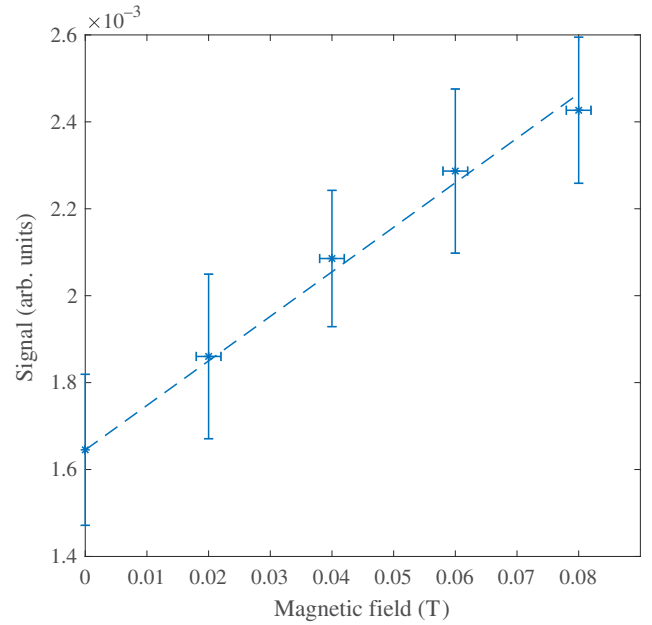

FIG. 4. Depolarization signal dependence on magnetic field strength. The trend is approximately linear, in agreement with our model. The zero magnetic field offset is due to other depolarization effects mentioned in the text. The vertical error bars represent the standard error in averaging each signal over the interval of 300–500 ns, while the horizontal error bars represent the uncertainty in the current dial controlling the magnetic field strength.

[9–16], and adjusting the receiver to magnetically induced depolarization to detect and measure magnetic fields.

The dependence of the depolarization scattering signal on external magnetic field strength is shown in Fig. 4. The magnetic field is varied by adjusting the current applied to the electromagnet. The trend is approximately linear, which is in agreement with our first-order model [Eq. (7)], and verifies that depolarization scattering is sensitive to the magnitude of the external magnetic field. A suitable calibration of this curve will allow quantitative measurements of the external magnetic field magnitude (since, in this case, $\mathbf{E}_0 \perp \mathbf{B}_{ext}$), or more generally for nonorthogonal fields, quantitative measurements of the external magnetic field component orthogonal to both $\mathbf{E}_0$ and the receiver polarization.

Since the depolarized signal has polarization in the $\mathbf{E}_0 \times \mathbf{B}_{ext}$ direction, reversing the magnetic field direction (in our case, by switching the current leads) should lead to a reversal of the magnetically induced dipole, which corresponds to a 180° phase shift in the depolarization signal. Figure 5 demonstrates this effect by varying the distance of the receiver from the small plasma and plotting the signals for both positive ($+\hat{\mathbf{z}}$) and negative ($-\hat{\mathbf{z}}$) polarity magnetic fields, with subtraction of the $B_{ext} = 0$ background signal. The horizontal axis is the phase difference between the scattered (rf) and local oscillator (LO) microwaves,
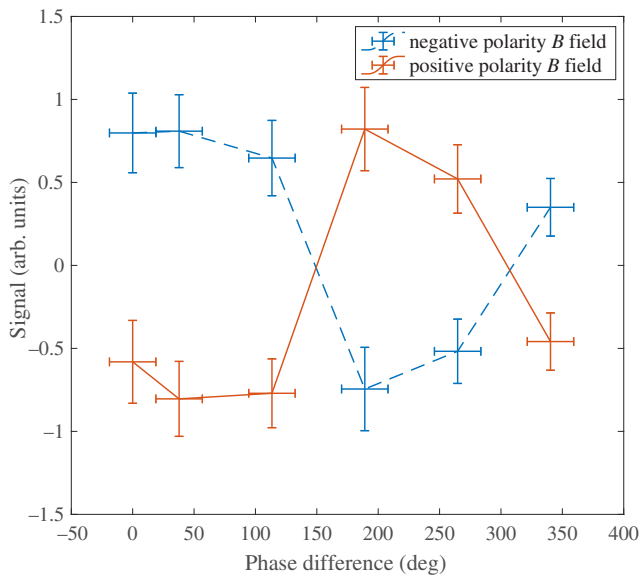
FIG. 5. Depolarization signal dependence on positive and negative polarity magnetic fields for varying phase difference between the rf and LO signals, corresponding to changing the receiver distance from the small plasma. We see a sinusoidal dependence for each signal, with a relative phase difference of 180° between the signals, corresponding to a sign reversal of the magnetically induced dipole. The vertical error bars are described in Fig. 4, while the horizontal error bars represent the uncertainty in the distance measurements due to ruler resolution.

which is calculated from normalizing the receiver displacement by λ and multiplying by 360°. We see a sinusoidal dependence for each signal, with a period of 360°, corresponding to a full-wavelength displacement between the rf and LO signals. The depolarization signals for positive and negative polarity external magnetic fields have a relative phase difference of 180°, which is a verification of the sign reversal predicted for the magnetically induced dipole and demonstrates the capability to detect magnetic field polarity.

V. CONCLUSION

In summary, we investigate the effect of an external magnetic field on microwave scattering from a laser-generated plasma, where we predict and detect a magnetically induced depolarization of the scattered microwaves. Scattering is localized at the small laser-generated plasma and depends on the magnitude and direction of the magnetic field, showing the potential for standoff detection and measurement of local vector magnetic fields. The standoff capability of the proposed measurement technology opens up the possibility of vector magnetic field measurements in limited diagnostic access environments. The nanosecond time resolution provides a time-resolved measurement of the magnetic field, which may be useful in monitoring

rapidly varying magnetic field fluctuations. Since depolarization and **E** polarization signals differ in their response to an external magnetic field, one can use this knowledge to either minimize magnetic field influence on a measurement quantity of interest, or maximize magnetic field influence to measure the local structure of the magnetic field. Although the small plasma is generated via REMPI in our case, in principle, any small plasma can be used. The magnetically induced depolarization effect can be extended to different regimes in the electromagnetic spectrum, such as terahertz or millimeter waves. Notably, the plasma should satisfy the Rayleigh regime if quantitative measurements are to be made, although a plasma in the Mie regime will also demonstrate the qualitative effect of magnetically induced depolarization, and hence, will still allow detection of the magnetic field.

[1] M. Faraday, I. Experimental researches in electricity.—Nineteenth series, Phil. Trans. R. Soc. Lond. **136,** 1 (1846).

[2] J. Kerr, XLIII. On rotation of the plane of polarization by reflection from the pole of a magnet, Phil. Mag. **3,** 321 (1877).

[3] W. Voigt, Uber das elektrische analogon des zeeman-effektes, Ann. Der Phys. **4,** 197 (1901).

[4] A. A. Dougal, J. P. Craig, and R. F. Gribble, Time-space Resolved Experimental Diagnostics of Theta-pinch Plasma by Faraday Rotation of Infrared He—Ne Maser Radiation, Phys. Rev. Lett. **13,** 156 (1964).

[5] Y. Geng, X. Wu, and L.-W. Li, Analysis of electromagnetic scattering by a plasma anisotropic sphere, Radio Sci. **38,** 1104 (2003).

[6] Y. Ahmadizadeh, B. Jazi, and A. Abdoli-Arani, Analysis of long wavelength electromagnetic scattering by a magnetized cold plasma prolate spheroid, Waves Random Complex Medium **23,** 336 (2013).

[7] A. K. Ram and K. Hizanidis, Scattering of electromagnetic waves by a plasma sphere embedded in a magnetized plasma, Radiat. Eff. Defects Solids **168,** 759 (2013).

[8] M. N. Shneider and R. B. Miles, Microwave diagnostics of small plasma objects, J. Appl. Phys. **98,** 033301 (2005).

[9] Z. Zhang, M. N. Shneider, and R. B. Miles, Coherent Microwave Rayleigh Scattering from Resonance-enhanced Multiphoton Ionization in Argon, Phys. Rev. Lett. **98,** 265005 (2007).

[10] A. Shashurin, M. N. Shneider, A. Dogariu, R. B. Miles, and M. Keidar, Temporary-resolved measurement of electron density in small atmospheric plasmas, Appl. Phys. Lett. **96,** 171502 (2010).

[11] A. Dogariu and R. B. Miles, Detecting localized trace species in air using radar resonance-enhanced multi-photon ionization, Appl. Opt. **50,** A68 (2011).

[12] A. Dogariu, M. N. Shneider, and R. B. Miles, Versatile radar measurement of the electron loss rate in air, Appl. Phys. Lett. **103,** 224102 (2013).

[13] Y. Wu, J. Sawyer, Z. Zhang, and S. F. Adams, Flame temperature measurements by radar resonance-enhanced multiphoton ionization of molecular oxygen, Appl. Opt. **51,** 6864 (2012).

[14] R. B. Miles, J. B. Michael, C. M. Limbach, S. D. McGuire, T. Chng, M. R. Edwards, N. J. DeLuca, M. N. Shneider, and A. Dogariu, New diagnostic methods for laser plasma- and microwave-enhanced combustion, Phil. Trans. R. Soc. A **373,** 0338 (2015).

[15] Y. Wu, M. Gragston, Z. Zhang, and J. D. Miller, Spatially localized, see-through-wall temperature measurements in a flow reactor using radar REMPI, Opt. Lett. **42,** 53 (2017).

[16] A. Sharma, M. N. Slipchenko, M. N. Shneider, X. Wang, K. A. Rahman, and A. Shashurin, Counting the electrons in a multiphoton ionization by elastic scattering of microwaves, Sci. Rep. **8,** 2874 (2018).

[17] S. J. Seltzer and M. V. Romalis, Unshielded three-axis vector operation of a spin-exchange-relaxation-free atomic magnetometer, Appl. Phys. Lett. **85,** 4804 (2004).

[18] V. I. Yudin, A. V. Taichenachev, Y. O. Dudin, V. L. Velichansky, A. S. Zibrov, and S. A. Zibrov, Vector magnetometry based on electromagnetically induced transparency in linearly polarized light, Phys. Rev. A **82,** 033807 (2010).

[19] B. Patton, E. Zhivun, D. C. Hovde, and D. Budker, All-optical Vector Atomic Magnetometer, Phys. Rev. Lett. **113,** 013001 (2014).

[20] T. Thiele, Y. Lin, M. O. Brown, and C. A. Regal, Self-calibrating Vector Atomic Magnetometry Through Microwave Polarization Reconstruction, Phys. Rev. Lett. **121,** 153202 (2018).

[21] L. D. Landau and E. M. Lifshitz, *Electrodynamics of Continuous Media* (Pergamon, Amsterdam, 1984).

[22] J. D. Jackson, *Classical Electrodynamics* (Wiley, New Jersey, 1998).

[23] S. Kacenjar, M. Hausman, M. Keskinen, A. W. Ali, J. Grun, C. K. Manka, E. A. McLean, and B. H. Ripin, Magnetic field compression and evolution in laser-produced plasma expansions, Phys. Fluids **29,** 2007 (1986).